1521-0111/94/4/1174–1186$35.00
MOLECULAR PHARMACOLOGY

https://doi.org/10.1124/mol.118.112631
Mol Pharmacol 94:1174–1186, October 2018

Compensatory Expression of Nur77 and Nurr1 Regulates NF-κB–Dependent Inflammatory Signaling in Astrocytes

Katriana A. Popichak, Sean L. Hammond, Julie A. Moreno, Maryam F. Afzali, Donald S. Backos, Richard D. Slayden, Stephen Safe, and Ronald B. Tjalkens

Departments of Environmental and Radiological Health Sciences (K.A.P., S.L.H., R.B.T.) and Microbiology, Immunology and Pathology (J.A.M., M.F.A., R.D.S.), College of Veterinary Medicine and Biomedical Sciences, Colorado State University, Fort Collins, Colorado; Department of Pharmaceutical Sciences, University of Colorado Anschutz Medical Campus, Aurora, Colorado (D.S.B.); and Department of Veterinary Physiology and Pharmacology, Texas A&M University, College Station, Texas (S.S.)

Received April 2, 2018; accepted August 1, 2018

ABSTRACT

Inflammatory activation of glial cells promotes loss of dopaminergic neurons in Parkinson disease. The transcription factor nuclear factor κB (NF-κB) regulates the expression of multiple neuroinflammatory cytokines and chemokines in activated glial cells that are damaging to neurons. Thus, inhibition of NF-κB signaling in glial cells could be a promising therapeutic strategy for the prevention of neuroinflammatory injury. Nuclear orphan receptors in the NR4A family, including NR4A1 (Nur77) and NR4A2 (Nurr1), can inhibit the inflammatory effects of NF-κB, but no approved drugs target these receptors. Therefore, we postulated that a recently developed NR4A receptor ligand, 1,1bis (3′indolyl) 1(pmethoxyphenyl) methane (C-DIM5), would suppress NF-κB-dependent inflammatory gene expression in astrocytes after treatment with 1-methyl-4-phenyl 1, 2, 3, 6-tetrahydropyridine (MPTP) and the inflammatory cytokines interferon γ and tumor necrosis factor α. C-DIM5 increased expression of Nur77 mRNA and suppressed expression of multiple neuroinflammatory genes. C-DIM5 also inhibited the expression of NFκB-regulated inflammatory and apoptotic genes in quantitative polymerase chain reaction array studies and effected p65 binding to unique genes in chromatin immunoprecipitation next-generation sequencing experiments but did not prevent p65 translocation to the nucleus, suggesting a nuclear-specific mechanism. C-DIM5 prevented nuclear export of Nur77 in astrocytes induced by MPTP treatment and simultaneously recruited Nurr1 to the nucleus, consistent with known transrepressive properties of this receptor. Combined RNAi knockdown of Nur77 and Nurr1 inhibited the anti-inflammatory activity of C-DIM5, demonstrating that C-DIM5 requires these receptors to inhibit NF-κB. Collectively, these data demonstrate that NR4A1/Nur77 and NR4A2/Nurr1 dynamically regulated inflammatory gene expression in glia by modulating the transcriptional activity of NF-κB.

Introduction

Parkinson disease (PD) is associated with selective degeneration of dopaminergic neurons within the substantia nigra pars compacta (SNpc) of the midbrain. The only available treatments are symptomatic, involving pharmacologic replacement or augmentation of dopamine. Patients become refractory to these interventions over time, however, owing to a continued loss of dopaminergic neurons, resulting in dose escalations and debilitating drug-induced dyskinesia (Jankovic, 2008; Panneton et al., 2010; Kalia and Lang, 2015). Observations made postmortem from the brains of individuals who suffered from PD indicate a sustained inflammatory response within microglia and astrocytes in the SNpc associated with damage to neurons and disease progression (Hirsch et al., 2003; Teismann and Schulz, 2004; Pekny and Nilsson, 2005; Pekny et al., 2014).

The transcription factor nuclear factor κB (NF-κB), an important regulator in microglia and astrocytes, modulates the expression of inflammatory genes associated with neuronal damage and disease progression in PD (Hirsch and Hunot, 2000; Hirsch et al., 2003; Teismann and Schulz, 2004; Béchade et al., 2014; Frakes et al., 2014). Pharmacologic and genetic inhibition of NF-κB in microglia and astrocytes can decrease activation, expression of neuroinflammatory genes, and neuronal cell death in glial-neuronal coculture models (Kirkley et al., 2017), as well as in animal models of PD, Alzheimer disease, and multiple sclerosis (Saijo et al., 2009; Liddelow et al., 2017; Rothe et al., 2017). NF-κB integrates multiple intracellular and extracellular stress signals through the IκBα kinase complex, causing translocation of the p50/p65 active transcription factor to the nucleus (Karin and Ben-Neriah, 2000); however, is not a tractable drug target given that knockout mice for this pathway

This work was supported by the National Institutes of Health (NIH) [Grants ES021656, ES026860, and ES025713], as well as a grant from the Consolidated Anti-Aging Foundation. Molecular modeling studies were supported by the NIH [Grant UL1 TR001082].
https://doi.org/10.1124/mol.118.112631.

ABBREVIATIONS: C-DIM5, di-indolylmethane (DIM)-C-pPhOCH3; ChIP-seq, chromatin immunoprecipitation next-generation sequencing; DMSO, dimethylsulfoxide; DsiRNA, dicer-substrate RNA; GFAP, glial fibrillary acidic protein; GFP, green fluorescent protein; GO, gene ontology analysis; HEK, human embryonic kidney cell line; IFNγ, interferon-γ; LPS, liposaccharide; MPTP, 1methyl4phenyl1, 2, 3, 6 tetrahydropyridine; NF-κB, nuclear factor κB; PBS, phosphate-buffered saline; PD, Parkinson disease; qPCR, quantitative polymerase chain reaction; RPKM, reads per kilobase million; siRNA, small interfering RNA; SNpc, substantia nigra pars compacta; TNFα, tumor necrosis factor α.

die in utero (Tanaka et al., 1999). More recently, it was reported that several nuclear receptors, including NR4A orphan receptors (nerve growth factor–induced-b receptors), can antagonize NF-κB signaling by stabilizing nuclear corepressor protein complexes at NF-κB *cis*-acting elements in the promoter regions of inflammatory genes in macrophages and microglia (Saijo et al., 2009, 2013; De Miranda et al., 2015a,b; McEvoy et al., 2017); however, no approved drugs target NR4A receptors.

Based on these findings, we reported that an activator of NR4A2 (Nurr1), the *phenyl* substituted di-indolylmethane derivative, 1,1bis(3′indolyl)1(*p*chlorophenyl) methane (CDIM12), prevented liposaccharide (LPS)-induced activation of NF-κB in BV-2 microglial cells by stabilizing the nuclear corepressor proteins CoREST, a corepressor for the repressor protein RE1 silencing transcription factor/neural-restrictive silencing factor (REST/NRSF), and HDAC at NF-κB binding sites in the promoter region of NOS2 (De Miranda et al., 2015a). Less is known about the anti-inflammatory activity of NR4A1 (Nur77), although a recent study demonstrated that loss of dopaminergic neurons induced by the neurotoxin 1-methyl-4-phenyl-1, 2,3,6-tetrahydropyridine (MPTP) is more severe in Nur77 knockout mice compared with wild-type mice and that MPTP-dependent downregulation of NR4A1 is associated with dysfunction in neuronal differentiation and development (St-Hilaire et al., 2006). It has also been reported that homeostatic and anti-inflammatory functions of NR4A receptors extend to maintenance of neurologic function and decreased injury in cardiovascular disease, as well as modulation of inflammatory immune responses in arthritis (Safe et al., 2015; McEvoy et al., 2017). Although recent studies suggest that NR4A1/Nur77 modulates LPS-induced inflammatory signaling in microglia (Chen et al., 2017), it is not known whether NR4A1/Nur77 has a similar function in modulating NF-κB–dependent inflammatory signaling in astrocytes.

We therefore postulated that a ligand for both Nur77 and Nurr1 [1,1bis (3′indolyl)1(*p*methoxyphenyl) methane (C-DIM5)] would suppress NF-κB–dependent inflammatory gene expression in astrocytes induced by treatment with MPTP and the inflammatory cytokines interferon γ (IFNγ) and tumor necrosis factor α (TNFα). C-DIM5 suppressed the expression of multiple NF-κB–regulated neuroinflammatory genes in primary astrocytes without preventing translocation of p65 to nucleus after an inflammatory stimulus. In addition, C-DIM5 increased nuclear localization of both Nur77 and Nurr1, suggesting a nuclear mechanism of action. Knockdown of either NR4A1/Nur77 or NR4A2/Nurr1 by RNA interference resulted in a compensatory increase in mRNA expression for the opposite receptor, but not for NR4A3/Nor1, indicating that these receptors are closely coregulated in astrocytes. Genome-wide chromatin immunoprecipitation (ChIP)/next-generation sequencing (ChIP-seq) analysis revealed that C-DIM5 modulates NF-κB/p65 transcription factor binding across multiple loci in astrocytes, including those regulating inflammation, cell division, and neuronal trophic support. Thus, we have demonstrated that pharmacologic modulation of NR4A receptors in glial cells may represent a promising approach to selectively inhibit glial inflammation in the prevention of neurotoxic and neuroinflammatory injury.

Materials and Methods

Materials. DIM-C-pPhOCH3 (C-DIM5) was synthesized by Dr. Stephen Safe and characterized as previously described (Qin et al., 2004), where the substitution of –OCH3 is what differentiates C-DIM5 from C-DIM12 (substitution is –Cl). All general chemical reagents, including cell culture media, antibiotics, and fluorescent antibodies and dyes, were purchased from Life Technologies (Carlsbad, CA) or Sigma-Aldrich (St. Louis, MO) unless otherwise stated. TNFα and IFNγ were purchased from R&D Systems (Minneapolis, MN). Monoclonal antibodies against Nurr1 and Nur77 were purchased from Santa Cruz Biotechnology (Santa Cruz, CA), and horseradish peroxidase–conjugated goat anti-mouse and goat anti-rabbit secondary antibodies were purchased from Cell Signaling (Danvers, MA). For immunofluorescence studies, antibodies against glial fibrillary acidic protein (GFAP), anti-FLAG, β-actin, and p65 were purchased from Sigma Chemical Co. and Santa Cruz Biotechnology, respectively. Antibodies used for ChIP analysis of p65 were purchased from Santa Cruz Biotechnology. Reagents used for transfection experiments were purchased from Mirus Bio (Madison, WI) for TransIT-X2 System reagent and Invitrogen (Carlsbad, CA) for LipofectAMINE reagent. The NF-κB-293T- green fluorescent protein (GFP)-Luc reporter (human embryonic kidney, HEK) cell line was purchased from System Biosciences (Mountain View, CA).

Primary Cell Isolation. Cortical glia were isolated from 1-day-old C57Bl/6 or transgenic mouse pups according to procedures described previously (Aschner and Kimelberg, 1991) and purity-confirmed through immunofluorescent staining using antibodies against GFAP and IBA1. For a brief explanation of primary cellular isolation, see Carbone et al. (2009). All animal procedures were approved by the Colorado State University Institutional Animal Care and Use Committee and were conducted in accordance with published NIH guidelines.

Gene Knockdown Assays. RNA interference (small interfering RNA, siRNA) sequences were acquired from Integrated DNA Technologies (IDT DNA, Coralville, IA). Nurr1 and Nur77 RNAi duplexes were designed against splice common variants of the target gene and were validated using a dose-response assay with increasing concentrations of the suspended oligo (900–1200 ng/ml) using a standard scrambled dicer-substrate RNA (DsiRNA) as control. Astrocytes were transfected with RNAi oligonucleotides using the TransIT-X2 delivery system (Mirus Bio) 48 hours before treatment with MPTP (10 μM), and the inflammatory cytokines TNFα (10 pg/ml) and IFNγ (1 μg/μl), with or without DIM-C-pPhOCH3 (C-DIM5) (10 μM) treatment or vehicle control (dimethylsulfoxide, DMSO), for 4 hours of separate siRNA systems were used to ensure specific knockdown of Nurr1 and Nur77 mRNA while limiting off-target effects on other nuclear receptor family members (Nur77 or Nurr1, respectively, and Nor1). The Nurr1 dsiRNA duplex sequences are (5′→3′) CUAGGUUGAA-GAUGUUAUAGGCACT; AGUGCCUAUAACAUCUUCAACCUAGAA (IDT DsiRNA; designated siNurr1) and the Nur77 DsiRNA duplex sequences (5′→3′) UCGUUGCUGGUGUUCCAUAUUGAGCUU; AGCAACGACCACAAGGUAUAACUCG (IDT DsiRNA; designated siNur77).

Flow Cytometry. The percentage of astrocytes in confluent mixed glial (astrocyte and microglia) cultures before and after transfections with siNur77 and/or siNurr1 were determined by immunophenotying using direct labeling with anti-GLAST-PE (Miltenyi Biotec, San Diego, CA) and anti-Cd11b-FITC (BD Biosciences, San Jose, CA), followed by flow cytometric analysis as described (Kirkley et al., 2017).

Real-Time Reverse Transcriptase-Polymerase Chain Reaction and Quantitative Polymerase Chain Reaction Arrays. Confluent glia were treated with MPTP (10 μM) and the inflammatory cytokines TNFα (10 pg/ml) and IFNγ (1 μg/μl), after a 1-hour pretreatment, with or without DIM-C-pPhOCH3 (C-DIM5) (1 or 10 μM) or a DMSO vehicle control, for 4 hours before RNA isolation. RNA was isolated using the RNEasy mini-kit (Qiagen, Valencia, CA), and purity and concentration were determined using a Nanodrop ND-1000 spectrophotometer (NanoDrop Technologies, Wilmington, DE). After purification, RNA (250–1000 ng) was used as template for reverse transcriptase reactions using the iScript RT kit (Bio-Rad Technologies, Hercules CA). The resulting cDNA was profiled for gene expression according to the 2-ΔΔCT method (Livak and Schmittgen,

2001). Primer sequences of additional genes profiled are presented in Table 1. Predesigned quantitative polymerase chain reaction (qPCR) arrays profiling NF-κB target pathway genes were purchased in a 384-well format from SA Biosciences (Frederick, MD) and processed according to the manufacturer's instructions using a Roche Light Cycler 480 (Indianapolis, IN). Array data were analyzed using an online software package accessed through SA Biosciences.

Western Blotting. Confluent glia were treated with MPTP (10 μM) and the inflammatory cytokines TNF-α (10 pg/ml) and IFN-γ (1 ng/ml), with or without DIM-C-pPhOCH3 (C-DIM5) (10 μM) or a DMSO vehicle control for 8 hours; or, to ensure effective overexpression of Nur77/NR4A1, NF-κB-293T-GFP-Luc reporter (i.e., HEK) cells were transfected for 24 hours with human-NR4A1-FLAG/FLAG-TRE or human-empty-FLAG before protein harvesting. Cells were lysed with RIPA buffer, quantified via Pierce BCA protein assay kit (Thermo Scientific, Waltham, MA), and combined with SDS-PAGE loading buffer (1× final concentration); equal volumes/total protein were separated by standard SDS-PAGE using a 10% acrylamide gel (BioRad) followed by semidry transfer to polyvinylidene fluoride membrane (Pall Corp., Pensacola, FL). All blocking and antibody incubations were performed in 5% nonfat dry milk in tris-buffered saline containing 0.2% Tween-20. Protein was visualized on film using enhanced chemiluminescence (Pierce, Rockford, IL) on a Chemidoc XRS imaging system (Bio-Rad). Membranes were stripped of antibody and reprobed against β-actin to confirm consistent protein loading among sample groups.

NF-κB Reporter Assays. For green fluorescent protein/49,6-diamidino-2-phenylindole (GFP/DAPI) and luminescence/protein expression assays, NF-κB-GFP/Luc reporter cells were grown in DMEM (Life Technologies) supplemented with 10% FBS and 1× PSN (as described earlier) on 96-well black-walled plates (Thermo Scientific). Cells were plated 24 hours before transfection with FLAG-TRE or Empty-FLAG with LipofectAMINE reagent for 24 hours before 24-hour treatment with 10 ng/ml TNFα, with or without 1 μM of C-DIM5. Cells were washed with 1× phosphate-buffered saline (PBS) and stained with Hoechst 33342 (Molecular Probes/Life Technologies, Eugene, OR) in Fluorobrite DMEM (Life Technologies) incubated at 37°C, 5% CO_2 for 5 minutes and then washed again with 1× PBS. The medium was replaced with fresh fluorobrite DMEM before reading the plate at 488/519 nm for GFP fluorescence expression and 345/478 nm for DAPI fluorescence expression on a Cytation3 cell imaging multimode reader (BioTek Instruments, Winooski, VT). GFP expression intensity values were divided over DAPI expression intensity values for quantitative analysis. Luciferase assays were run according to the protocol provided by the luciferase assay kit used in which Bright-Glo lysis buffer (Promega, Madison, WI) was added after PBS wash; additionally, total protein was ascertained via BCA assay. Chemiluminescence was also detected on a Cytation3 plate reader. All chemiluminescent values were divided over total amount of protein (micrograms per milliliter) for quantitative analysis.

Immunofluorescence Microscopy of Nurr1 (hNR4A1), Nur77, and p65 Shuttling. Primary astrocytes or hNR4A1-FLAG–transfected human embryonic kidney (HEK) cells were grown to confluence on 20-mm serum-coated glass coverslips and treated with saline or MPTP (10 μM), TNF-α (10 pg/ml), IFN-γ (1 ng/ml) for glia, or TNF-α (10 ng/ml) for transfected HEK cells, with or without DIM-C-pPhOCH3 (C-DIM5) (1 or 10 μM), or a DMSO vehicle control for a time course of 24 hours for p65 and transfected HEK cells, and then 30 minutes for remaining immunofluoresence in glia. Blocking and antibody hybridization was conducted in 1% goat/donkey serum in PBS, and all washes were conducted in PBS. Coverslips were mounted in Vectashield mounting medium containing DAPI (Vector Laboratories, Burlingame, CA). Slides were imaged using a Zeiss Axiovert 200 M inverted fluorescence microscope encompassing a Hammamatsu ORCA-ER–cooled charge-coupled device camera (Hammamatsu Photonics, Hamamatsu City, Japan) using Slidebook software (version 5.5; Intelligent Imaging Innovations, Denver, CO), and six to eight microscopic fields were examined per treatment group over no less than three independent experiments. Quantification of protein was determined by measuring the fluorescence intensity of p65, Nurr1, Nurr7, GFP, or FLAG expression within the boundary of each cell, assisted by DAPI counterstain, and segmented using Slidebook 5.0 software function for fluorescence intensity minus background (F/F_o).

ChIP/Next-Generation Sequencing. Primary mixed glia were grown to confluence in 10-cm tissue culture plates (approximately 2×10^7cells) and treated 30 minutes with MPTP (10 μM) and the inflammatory cytokines TNF-α (10 pg/ml) and IFN-γ (1 ng/ml), with or without DIM-C-pPhOCH3 (10 μM), or a DMSO vehicle control before cross-linking with 1% formaldehyde (Thermo Scientific) for 10 minutes. The remaining steps were adapted from the Chromatrap ChIP protocol from the Chromatrap Pro-A Premium ChIP Kit (Chromatrap, Wrexham, UK). DNA was sheared into approximately

TABLE 1

Primer table.

Primer sequences of measured genes in qPCR experiments separate from the SABiosciences NF-κB-targeted gene array.

Gene	Accession No.	Primer Sequence (5′-3′)	Length
NOS2	NM_010927.3	For: TCA CGC TTG GGT CTT GTT	*bp*
		Rev: CAG GTC ACT TTG GTA GGA TTT	149
TNFα	NM_013693.3	For: CTT GCC TGA TTC TTG CTT CTG	140
		Rev: GCC ACC ACT TGC TCC TAC	
IL-1β	NM_008361.3	For: GCA GCA GCA CAT CAA CAA G	90
		Rev: CAC GGG AAA GAC ACA GGT AG	
NURR1/NR4A2	NM_001139509.1	For: GTG TTC AGG CGC AGT ATG G	153
		Rev: TGG CAG TAA TTT CAG TGT TGG T	
CCL2	NM_011331.2	For: TTAAAAACCTGGATCGGAACCAA	121
		Rev: GCATTAGCTTCAGATTTACGGGT	
CCL5	NM_013653.3	For: GCT GCT TTG CCT ACC TCT CC	104
		Rev: TCG AGT GAC AAA CAC GAC TGC	
IL-6	NM_031168.1	For:CTG CAA GAG ACT TCC ATC CAG	131
		Rev:AGT GGT ATA GAC AGG TCT GTT GG	
β-ACTIN	NM_007393.3	For: GCT GTG CTA TGT TGC TCT AG	117
		Rev: CGC TCG TTG CCA ATA GTG	
HPRT	NM_013556.2	For: TCA GTC AAC GGG GGA CAT AAA	142
		Rev: GGG GCT GTA CTG CTT AAC CAG	
NOR1/NR4A3	XM_006537657.3	For: TGC GTG CAA GCC CAG TAT AG	60
		Rev: ATA AGT CTG CGT GGC GTA AGT	
NUR77/NR4A1	NM_010444.2	For: TTG GGG GAG TGT GCT AGA AG	202
		Rev: GTA GGC TTG CCG AAC TCA AG	

500-bp fragments before removing 10% (200 ng) for input controls, and 2 mg of chromatin was loaded into the immunoprecipitation reaction with 2 mg of precipitating antibody (as suggested by Chromatrap) anti-p65 (372) from Santa Cruz Biotechnology.

Next-generation sequencing was performed by the Infectious Diseases Research Center Next Generation-Sequencing Core at Colorado State University using the Applied Biosystems (Foster City, CA) SOLiD 3 Plus System. Fragment-sequencing library preparation was performed by the Next Generation Sequencing Core accordinhg to standard SOLiD protocols (http://solid.appliedbiosytems.com). Each sample was deposited on a quadrant of the sequencing slide to achieve a bead density of ~65,000 beads per quadrant. Sequencing was conducted resulting in 35-bp reads that were filtered for high quality and aligned to the reference genome (GenBank). Reference genome alignments of the resulting ChIP-seq tags file provided the specific regions of protein binding in the genome.

ChIP Sequence Analysis of p65 DNA Binding. ChIP-Seq reads were mapped to the mouse genome (v10mm) using StrandNGS software. The raw reads were aligned with minimum of 90% identity, a maximum of 5% gaps, and 30 bp as the minimum aligned read length. Postalignment, peak detection was detected using PICS algorithm. A significant peak located in a window size of 250 bases per gene. Duplicates were filtered to avoid redundancy. Using StrandNGS software, gene ontology analysis was performed, and unique terms were determined using a cutoff of $P < 0.05$, enabling identification of the cellular processes that these unique genes are associated with in a particular treatment. Numbers of genes associated with each significant term were also noted (Boos and Stefanski, 2011).

Modeling. Molecular modeling was performed at the Computational Chemistry and Biology Core Facility at the University of Colorado Anschutz Medical Campus. All molecular modeling studies were conducted using Accelrys Discovery Studio 4.5 (Accelrys Inc., San Diego, CA), and the crystal structure coordinates for the NR4A1 and NR4A2 ligand binding domains (PDB IDs: 1OVL, 1YJE) (Wang et al., 2003; Flaig et al., 2005) were downloaded from the protein data bank (http://www.rcsb.org/pdb). The protein was prepared and subjected to energy minimization using the conjugate gradient minimization protocol with a CHARMm forcefield (Brooks et al., 2009) and the Generalized Born implicit solvent model with simple switching (Feig et al., 2004) that converged to a room mean square gradient of <0.01 kcal/mol. The Flexible Docking protocol (Koska et al., 2008), which allows flexibility in both the protein and the ligand during the docking calculations, was used to predict the c-DIM-5 binding mode in either the ligand binding site of NR4A1 or the coactivator binding pocket of NR4A2. Predicted binding poses were energy-minimized in situ using the CDOCKER protocol (Wu et al., 2003) before final ranking of docked poses via consensus scoring that combined the Jain (1996) PLP (Parrill and Reddy, 1999), and Ludi (Böhm, 1994) scoring functions. Interaction energies were calculated using implicit distance-dependent dielectrics.

Statistical Analysis. Experiments were performed no less than three times, with replicates consisting of independent cultures using a minimum of four plates or coverslips per replicate study. Comparison of two means was performed by Student's *t* test, and comparison of three or more means was performed using one-way analysis of variance followed by the Tukey-Kramer multiple comparison post hoc test using Prism software (v6.0h; Graphpad Software, Inc., San Diego, CA). For all experiments, data were reported as S.E.M. (±S.E.M.), and $P < 0.05$ was considered significant, although the level of significance was often much greater ($^*P < 0.05$; $^{**}P < 0.01$; $^{***}P < 0.001$; $^{****}P < 0.0001$).

Results

C-DIM5 Reduces NF-κB–Mediated Inflammatory Gene Expression in Primary Mixed Glial Cultures. The purity of mixed glial cultures was assessed by flow cytometry (Fig. 1A), demonstrating the cellular composition to be 78.8% astrocyte (Glast PE+) and 12.0% microglia (Cd11b FITC+). Primary culture mixed glia was treated with MPTP (10 μM) and cytokines TNFα (10 pg/ml) and IFNγ (1 ng/ml) or C-DIM5 (10 μM) alone for 24 hours and mRNA expression of Nr4a1/Nur77 and Nr4a2/Nurr1, as well as multiple inflammatory cytokines and chemokines, was assessed by real-time qPCR (Fig. 1, B and C). Nur77 mRNA levels were strongly induced by treatment with MPTP + TNF/IFN by 4 hours. Treatment with C-DIM5 (10 μM) also induced expression of Nur77 mRNA by approximately 20-fold over control and combined treatment with both MPTP + TNF/IFN further increased expression of Nur77 mRNA by approximately 40-fold over control (Fig. 1B, right). In contrast, there was little or no increase in expression of Nurr1 mRNA with either treatment group (Fig. 1C). After treatment with MPTP + TNF/IFN, levels *of Nos2, Ccl2, Il6*, and *Tnf* peaked at 4 hours, and levels of *Ccl5* mRNA were maximal at 24 hours posttreatment compared with control (Fig. 1D, red). Treatment with C-DIM5 alone did not significantly increase the expression of any cytokines or chemokines examined (Fig. 1D, blue), whereas 4 hours of combined treatment with MPTP + TNF/IFN and C-DIM5 strongly suppressed mRNA expression of all inflammatory genes examined (Fig. 1E). To determine whether the observed inhibitory effect of C-DIM5 on transcript levels also occurred at a protein level, several NF-κB–regulated secreted cytokines were measured in the media of mixed glial cultures by multiplex enzyme-linked immunosorbent assay after 24-hour treatment with MPTP + TNF/IFN in the presence or absence of C-DIM5 or vehicle control (DMSO). As shown in Table 2, treatment of primary mixed glia with MPTP + TNF/IFN caused an increase in the inflammatory cytokines and chemokines IL6, IL-12p70, MIP-1a, CCL5, and CCL 17/TARC, with a trend toward increasing levels of IL2 as well. Cotreatment with C-DIM5 inhibited expression of each cytokine or chemokine examined.

C-DIM5 Inhibits NF-κB Activity through a Nuclear Specific Mechanism. To examine the capacity of C-DIM5 to functionally inhibit NF-κB-dependent gene expression, immortalized HEK cells stably expressing an NF-κB-GFP-luciferase reporter were transfected with a construct to overexpress FLAG-tagged human NR4A1/Nurr7/TRE (hNR4A1-FLAG, Fig. 2A). HEK cells transfected with a control vector containing only FLAG expressed very low amounts of endogenous Nur77 protein, which was highly overexpressed in cells transfected with the NR4A1-FLAG construct (Fig. 2A). The subcellular localization of transfected hNR4A1-FLAG was examined in HEK reporter cells by immunofluorescence to determine the effect of treatment with inflammatory cytokines and C-DIM5 on expression of this receptor (Fig. 2B). In HEK cells transfected with hNR4A1-FLAG, treatment with 30 ng/ml TNF caused increased the expression of NF-κB-GFP and Nur77 compared with control. Treatment with TNF in the presence of C-DIM5 or treatment with C-DIM5 alone maintained expression of Nur77 and reduced NF-κB–dependent expression of GFP. In contrast, HEK cells transfected with the control FLAG vector showed high expression levels of GFP after treatment with TNF (Fig. 2B). Expression of both NF-κB-Luc and NF-κB-GFP was quantified in Fig. 2, C and D. Treatment with TNF strongly induced expression of both NF-κB-Luc and NF-κB-GFP that was not inhibited by C-DIM5 except in cells, which overexpressed Nur77 (Fig. 2, C and D) demonstrating that the inhibitory response was both ligand- and

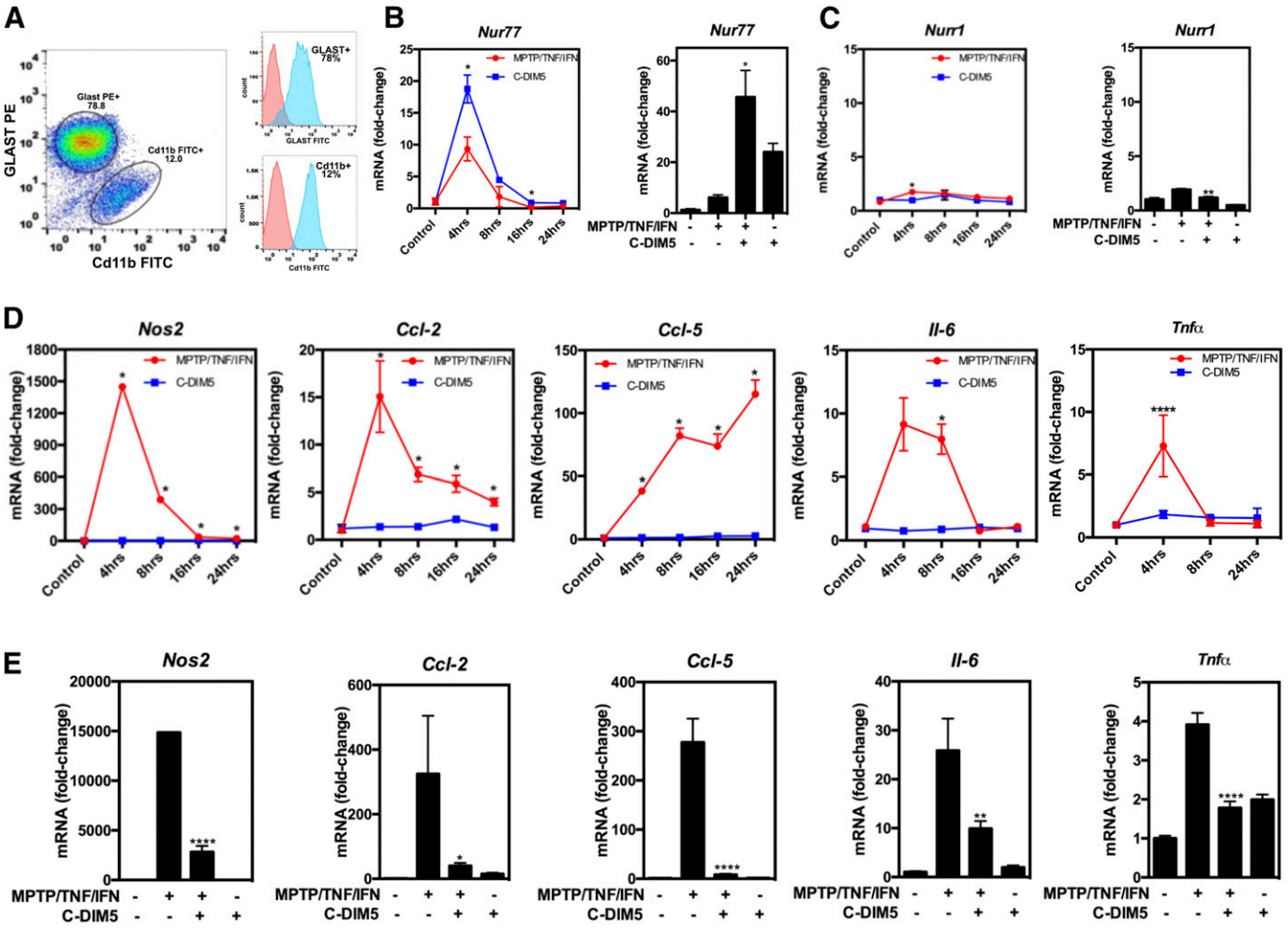

Fig. 1. C-DIM5 alone and MPTP/IFNγ/TNFα-induced mRNA expression in primary mixed glia over 24 hours. (A) Flow cytometry scatter plots show the percentage of Cd11b (microglia, 12%) or GLAST-positive (astrocytes, 78.8%) cells in mixed glial cultures. (B) C-DIM5 alone increases *Nur77* mRNA at 4 hours and MPTP/IFNγ/TNFα mildly activates *Nur77*; both synergistically show an increase. (C) C-DIM5 alone does not increase *Nurr1*. (D) Time course over 24 hours demonstrates the most inflammatory gene expression at 4 hours, whereas C-DIM5 does not. (E) C-DIM5 suppresses inflammatory gene expression at 4 hours. Data depicted as ±S.E.M. (n = 3–14); mRNA fold change; internal control (β-actin or HPRT). Statistical significance shown as mean compared with control except for those depicted in 2E, where statistical significance is compared with MPTP/TNF/IFN. *$P < 0.05$; **$P < 0.01$; ****$P < 0.0001$.

receptor-dependent. To determine whether C-DIM5 inhibited nuclear translocation of NF-κB/p65, the mean fluorescence intensity of nuclear p65 was determined by immunofluorescence after treatment with MPTP + TNF/IFN in the presence and absence of C-DIM5. MPTP + TNF/IFN induced rapid movement of p65 to the nucleus of astrocytes within 30 minutes of treatment that was not inhibited by C-DIM5 (Fig. 2E). Representative immunofluorescence images of astrocytes with p65 (red) and GFAP (green) are presented in Fig. 2F.

C-DIM5 Stabilizes Nuclear Localization of Both Nur77 and Nurr1 in Primary Astrocytes. Given that C-DIM5 increased *Nur77* mRNA expression with MPTP + TNF/IFN treatment and inhibited expression of multiple neuroinflammatory genes without preventing nuclear translocation of NF-κB, we assessed the effect of treatment with C-DIM5 on the subcellular localization of Nur77 and Nurr1 by immunofluorescence microscopy (Fig. 3). In astrocytes treated with MPTP + TNF/IFN, Nur77 translocated from the nucleus

TABLE 2

Reduction in secreted cytokines by C-DIM5

Inflammatory cytokines secreted upon MPTP/IFNγ/TNFα treatment are significantly reduced upon addition of C-DIM5.

Group	Secreted Cytokine Concentration (pg/ml)						TARC
	IL2	IL6	IL-12p70	CCL2	MIP-1a	CCL5	
Control	—	1.9 ± 0.65*	-**	13.2 ± 0.67**	-*	5.7 ± 0.52**	9.6 ± 0.47*
MPTP/TNF/IFN	3.1 ± 0.24	84.6 ± 1.13	7.4 ± 0.33	750.4 ± 7.58	4.1 ± 1.09	1916 ± 153.55	18.4 ± 0.80
MPTP/TNF/IFN + C-DIM5	2.6 ± 0.15	55.1 ± 2.53**	2.4 ± 0.27**	279.5 ± 5.74**	—*	111.2 ± 3.08**	16.6 ± 1.46*

—, Result lower than limit of detection.
*$P < 0.01$; **$P < 0.001$ Statistical significance from MPTP/TNF/IFN group (n = 4/group).

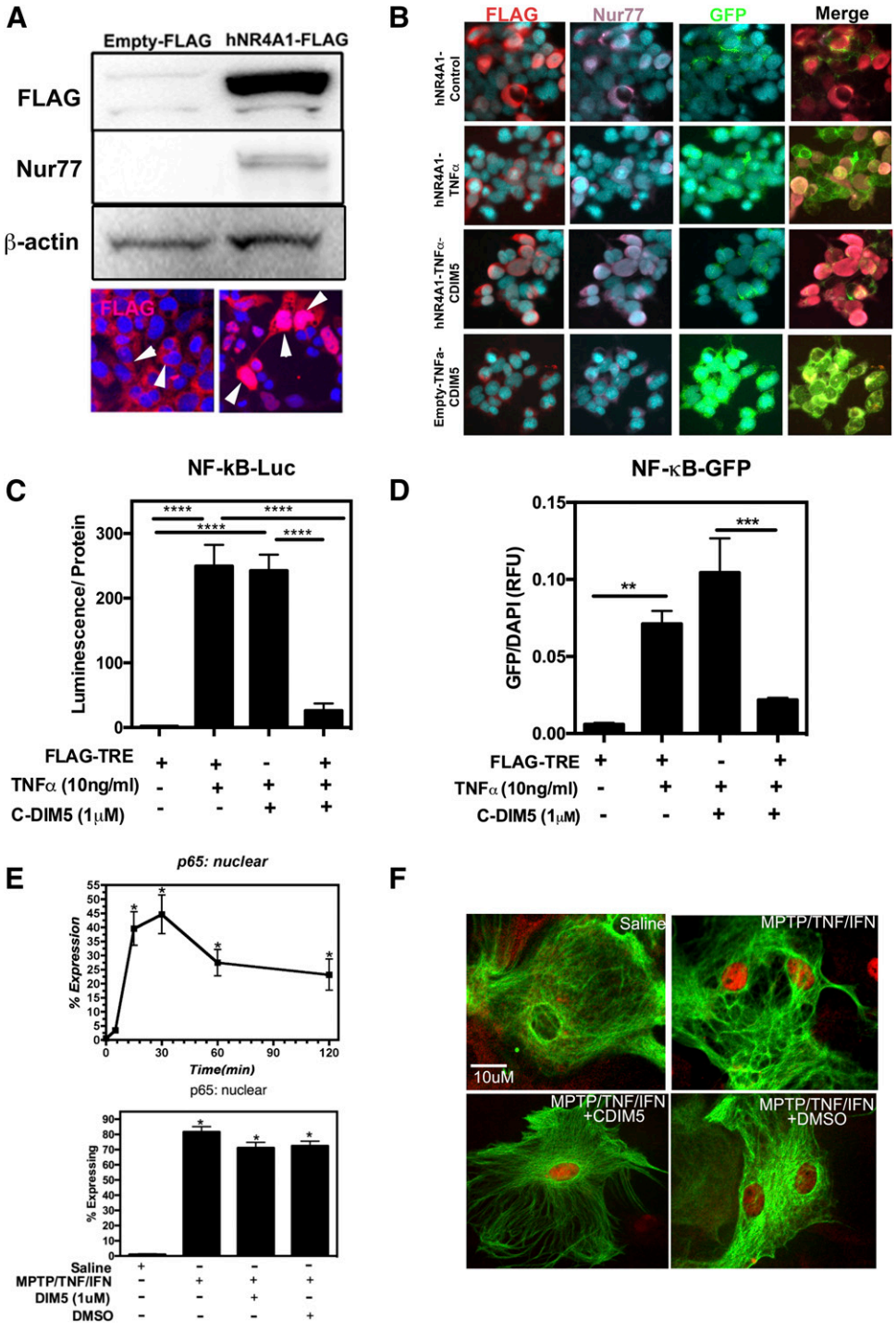

Fig. 2. C-DIM5 inhibits NF-κB activity in HEK NF-κB-GFP/luciferase reporter cells upon hNR4A1-FLAG (Nur77) overexpression through a nuclear specific mechanism exhibited in primary astrocytes. (A) Western blot and representative images demonstrating increased (arrows) Nur77 and FLAG in HEK dual-reporter cells. (B) Representative images demonstrating increased nuclear Nur77 upon overexpression in the presence of C-DIM5 after TNF treatment in HEK cells. (C and D) Quantitative graphs demonstrate decreased NF-κB activity via luciferase and GFP expression. (E) A time-course graph demonstrating increased nuclear p65 expression under the influence of MPTP and IFNγ/TNFα at 30 minutes in primary astrocytes. Additionally, C-DIM5 does not suppress p65 translocation. (F) Representative images of p65 translocation in astrocytes under basal conditions and/or stimulation with MPTP (10 μM) and TNF-α (10 pg/μl)/IFN-γ (1 ng/μl) in the absence or presence of 1 μM C-DIM5. Data depicted as ±S.E.M $^{*}P < 0.05$; $^{**}P < 0.01$; $^{***}P < 0.001$; $^{****}P < 0.0001$ n = 100–200 cells per group from three biologic replicates across three independent experiments.

to cytoplasm, whereas treatment with C-DIM5, alone or in the presence of MPTP + TNF/IFN, kept Nur77 sequestered in the nucleus (Fig. 3, A and B), as observed in HEK cells (Fig. 2B). In control astrocytes, Nurr1 was largely present in the cytoplasm. Treatment with MPTP + TNF/IFN caused a modest but significant increase in nuclear levels of Nurr1; however, treatment with C-DIM5 resulted in marked increase of nuclear Nurr1, irrespective of inflammatory stimulus (Fig. 3, C and D).

Modulation of NF-κB–Regulated Inflammatory Genes in Primary Glia by C-DIM5 Involves Compensatory Regulation of Nur77 and Nurr1. Previous studies demonstrated that C-DIM5 activates Nur77 to modulate gene transcription in pancreatic cancer cells (Yoon et al., 2011). We also reported that a chlorinated diindolylmethane analog of C-DIM5, 1,1-bis (3′-indolyl)-1-(p-chlorophenyl) methane (C-DIM12), effectively suppressed LPS-induced NF-κB signaling in BV-2 microglial cells by stabilizing transcriptional corepressor protein complexes at p65 binding sites on inflammatory gene promoters (De Miranda et al., 2015a) in a Nurr1-dependent manner. Based on these findings, we postulated that the observed inhibition of inflammatory gene expression in primary astrocytes treated with C-DIM5

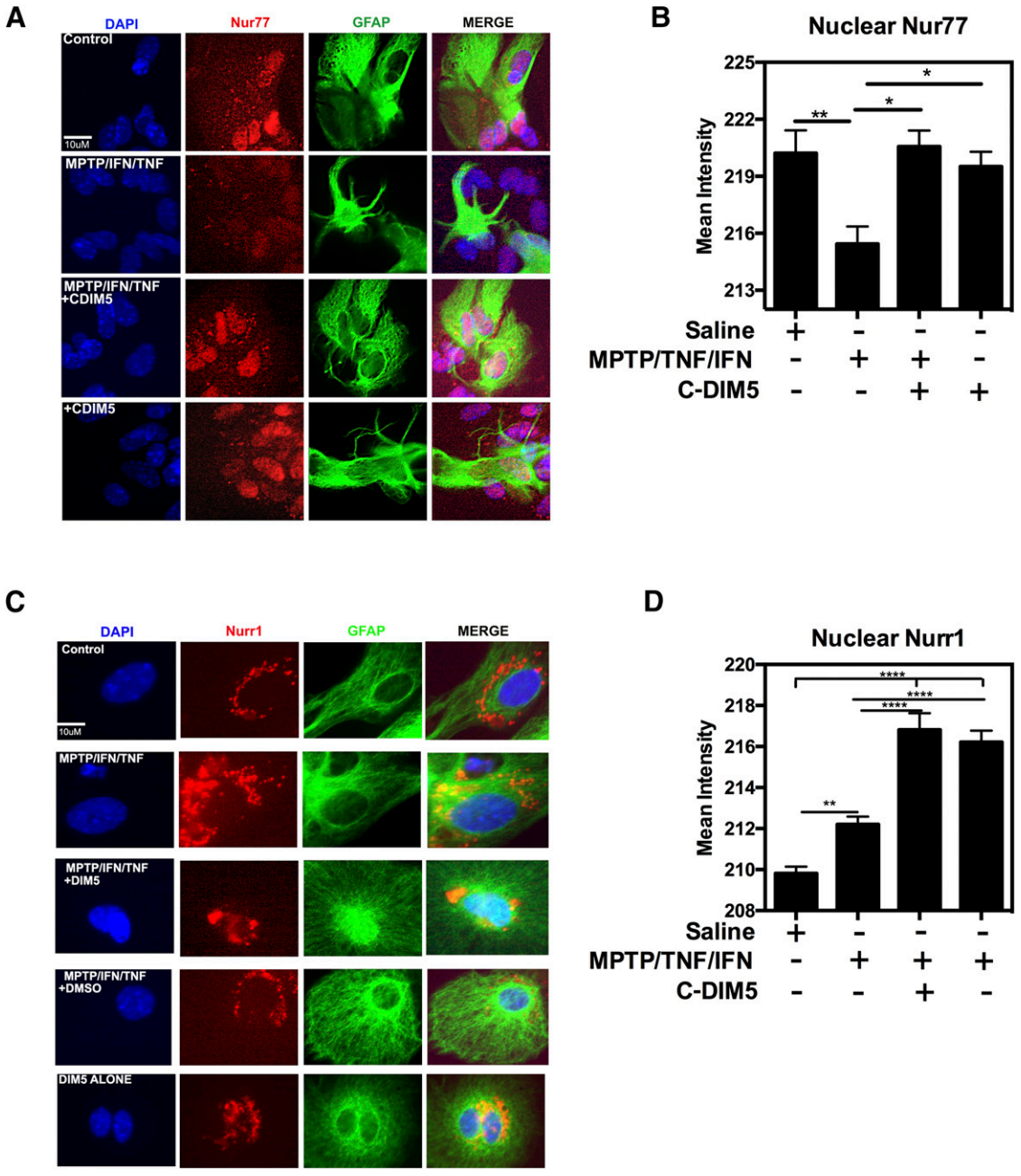

Fig. 3. C-DIM5 prevents Nur77 (NR4A1) from translocating to the cytoplasm and shuttles Nurr1 (NR4A2) to the nucleus under inflammatory stimuli. (A) Representative images of Nur77 translocation in astrocytes under control (saline) conditions and/or stimulation with MPTP/IFNγ/TNFα in the absence or presence of C-DIM5. (B) A quantitative figure demonstrating nuclear Nur77 expression at time point 30 minutes upon inflammatory stimuli and/or C-DIM5 treatment. (C) Representative images of Nurr1 translocation in astrocytes under control (saline) conditions and/or stimulation with MPTP/IFNγ/TNFα in the absence or presence of C-DIM5. (D) A quantitative figure demonstrating nuclear Nurr1 expression at time point 30 minutes upon inflammatory stimuli and/or C-DIM5 treatment or DMSO-vehicle control treatment. Data depicted as ±S.E.M $^*P < 0.05$; $^{**}P < 0.01$; $^{****}P < 0.0001$ n = 100–200 cells per image field per group for n = 3 across three independent experiments.

involved activation of Nur77 that subsequently inhibited expression of NF-κB–regulated inflammatory genes. To test this hypothesis, we used RNAi to sequentially knock down expression of Nur77 and Nurr1 in primary astrocytes and then examined the capacity of C-DIM5 to inhibit the expression of several NF-κB–regulated inflammatory cytokines and chemokines (Fig. 4). Expression of each NR4A family member was examined after RNAi directed against either Nur77 or Nurr1. After transfection of primary astrocytes with siRNA oligonucleotides directed against *Nr4a1/Nur77,* mRNA levels were reduced by ~90%, *Nr4a3/Nor1* mRNA was unaffected, whereas mRNA levels of *Nr4a2/Nurr1* doubled (Fig. 4A). Similarly, knockdown of Nr4a2/*Nurr1* had no effect on *Nor1/Nr4a3* mRNA but caused a compensatory increase in *Nr4a1/Nur77* mRNA levels 4-fold (Fig. 4B). Double knockdown of both *Nur77* and *Nurr1* effectively reduced mRNA for both receptors by ~60% (Fig. 4C) without affecting expression of *Nor1* (data not shown). We next examined protein expression of Nur77 and Nurr1 in highly purified cultures of astrocytes. After removal

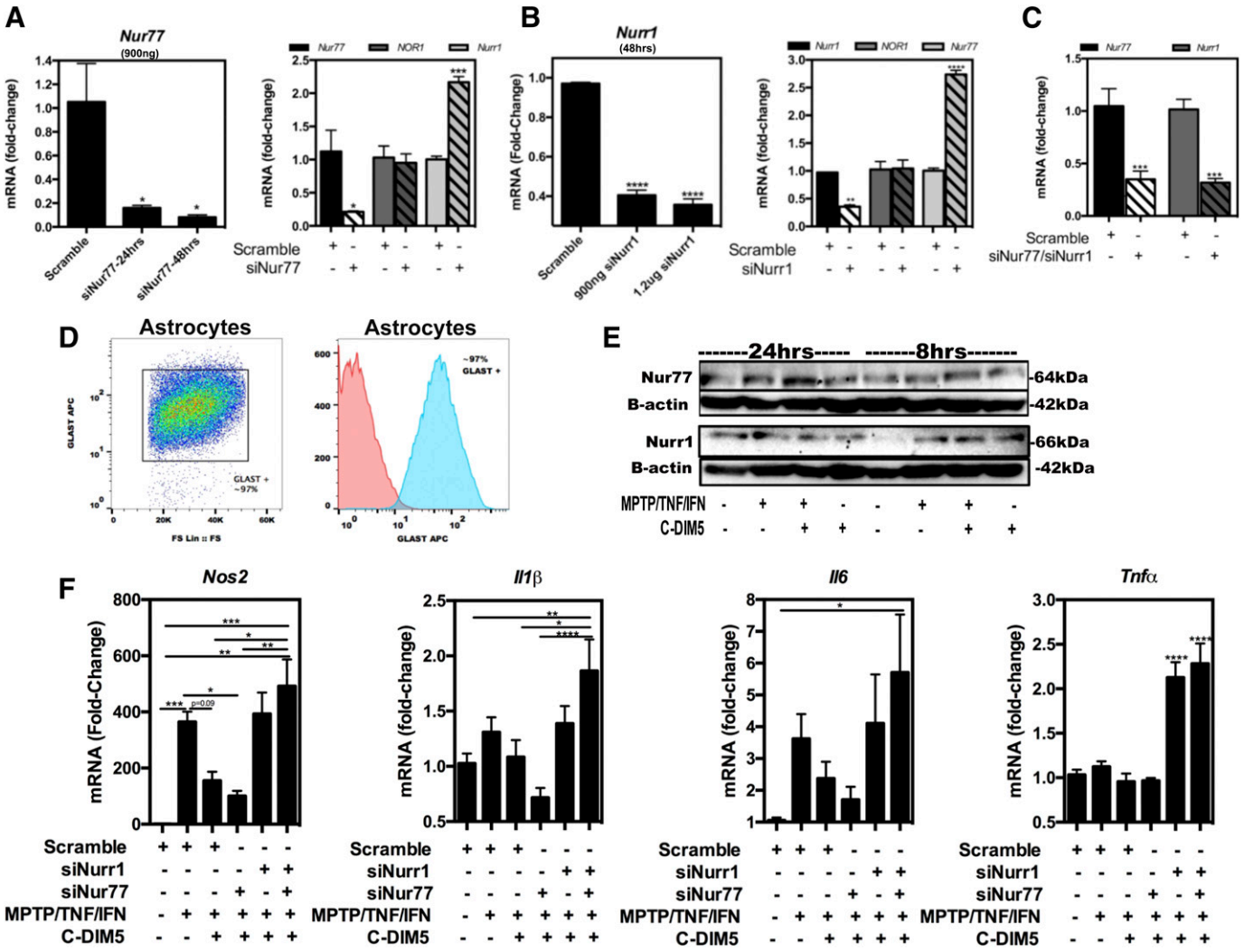

Fig. 4. RNAi targeted toward Nur77 and Nurr1 effectively knocks down Nur77 and Nurr1 mRNA expression in primary pure astrocytes, respectively. (A) Nur77 is silenced alone at 48 hours, which selectively increases expression of NR4A2/Nurr1 without affecting expression of NR4A3/NOR1. (B) Nurr1 is silenced alone, which selectively increases expression of NR4A1/Nur77 without affecting expression of NR4A3/NOR1 (C) Double knockdown of both Nur77 and Nurr1 effectively suppresses Nur77 and Nurr1, respectively. (D) Transfecting primary mixed glia effectively removes microglia yielding pure GLAST-positive primary astrocytes, as demonstrated by flow cytometry. (E) Twenty-four hour treatment with C-DIM5 alone or with MPTP-cytokines shows increased Nur77 protein compared with less Nurr1 protein. C-DIM5 effectively increases Nur77 at 24 hours versus 8 hours, whereas Nurr1 expression is expressed more at 8 hours. (F) Double knockdown prevents *Nos2, Il1β, Il6,* and *Tnfα* suppression by C-DIM5 with MPTP-cytokines. Data depicted as ±S.E.M. (n = 4–22/group); mRNA fold change; internal control (β-actin or HPRT). Statistical significance shown as mean compared with control. $^{*}P < 0.05$; $^{**}P < 0.01$; $^{***}P < 0.001$; $^{****}P < 0.0001$.

of microglial cells owing to transfection-induced microglial cell death, flow cytometric analysis indicated that cultures were >97% pure astrocytes based on immunoreactivity for the high-affinity glutamate transporter SLC1A3/GLAST (Fig. 4D). After 24-hour treatment with C-DIM5, protein levels of Nur77 were more robustly increased over control than were levels of Nurr1 (Fig. 4E). Astrocytes were next transfected with control siRNA oligonucleotides or siRNA oligonucleotides directed against Nur77 or Nurr1 singly (KD) or in combination (double KD) for 48 hours and then examined for expression of the NF-kB–regulated inflammatory genes *Nos2*, *Il1b*, *Il6*, and *Tnf* after inflammatory stimulus with MPTP + TNF/IFN for 4 hours in the presence or absence of C-DIM5 (Fig. 4F). In pure astrocyte cultures transfected with control siRNA and treated with MPTP + TNF/IFN, C-DIM5 inhibited expression of *Nos2* mRNA but had little inhibitory effect on expression of mRNA for *Il1b*, *Il6*, and *Tnf* compared with KD of *Nur77* alone, which enhanced suppression of mRNA expression for each gene examined after C-DIM5 treatment, whereas *Nurr1* KD alone resulted in little to no change in inflammatory gene expression on C-DIM5 treatment; however, double KD of both *Nur77* and *Nurr1* completely abolished the capacity of C-DIM5 to suppress inflammatory gene expression of *Nos2*, *Il1b*, *Il6*, and *Tnf* after treatment with MPTP + TNF/IFN (Fig. 4F, last bar in each graph).

ChIP-Seq and qPCR Array Analysis in Primary Astrocytes Demonstrates that C-DIM5 Transcriptionally Modulates the Expression of Multiple Genes Regulating Inflammation, Cell Death, and Neuronal Trophic Support. To identify unknown genes that interact with p65 in astrocytes in response to C-DIM5 during inflammatory activation, we conducted a genome-wide analysis of p65 binding to NF-κB consensus sequences of annotated genes in the mouse genome using ChIP-Seq (Fig. 5). By investigating

regions of the genome bound by p65 in cells treated with MPTP + TNF/IFN plus DMSO (vehicle control) in comparison with cells treated with MPTP + TNF/IFN plus C-DIM5, we identified 34 loci bound to p65 in both treatment groups, 36 unique loci bound to p65 in the MPTP + TNF/IFN vehicle control group (DMSO), and 21 loci bound to p65 unique to cells treated with MPTP + TNF/IFN + C-DIM5 (Fig. 5A). The loci bound to p65 that are statistically significant ($P < 0.05$) and unique to the C-DIM5–treated group correspond to numerous pathways important for neuronal function and survival,

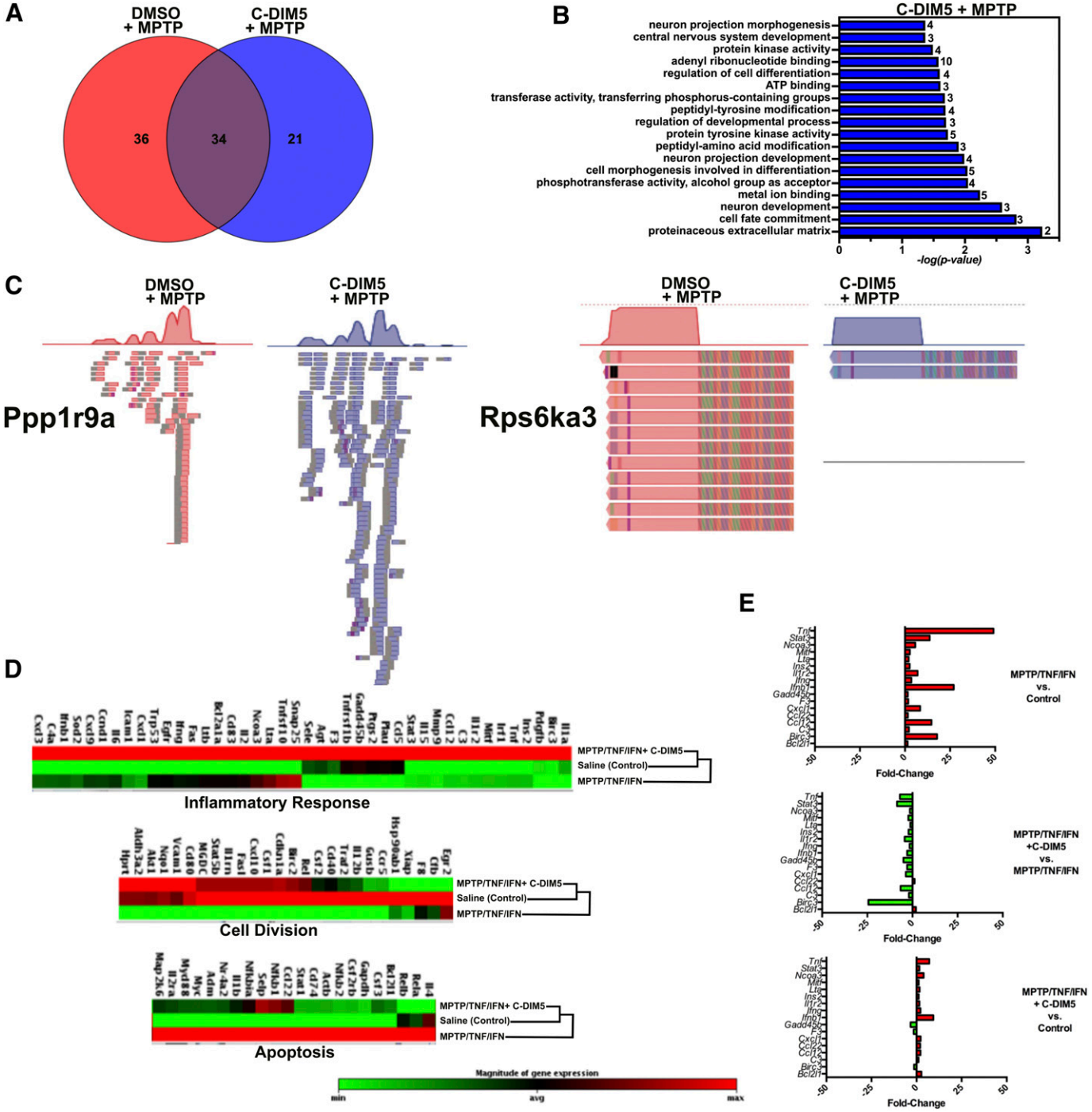

Fig. 5. ChIP-seq analysis of p65-bound genes in C-DIM5-treated MPTP-exposed astrocytes. C-DIM5 largely restores NF-κB-mediated inflammatory and apoptosis gene expression back to control levels as measured by a qPCR array study. (A) Venn diagram depicting unique and overlapping genes bound to p65 in C-DIM5 and vehicle (DMSO)-treated MPTP exposed astrocytes. (B) Bar plot for the gene ontology analysis of biologic processes found to be statistically unique in the C-DIM5-treated MPT-exposed astrocytes. –log(*P* value) used to rank the degree of enrichment of the top 21 genes. The number next to each bar represents the number of associated genes corresponding to C-DIM5–treated MPTP-exposed astrocytes. (C) Genome browser view of distribution of the ChIP-seq reads of represented genes in both C-DIM5- and DMSO-treated MPTP-exposed astrocytes. (D) A cluster gram and heat map demonstrate gene pattern expression similarities among treatment groups, MPTP/IFNγ/TNFα + C-DIM5 clusters with control (saline) levels; MPTP/IFNγ/TNFα clusters alone. (E) MPTP/IFNγ/TNFα increases gene expression from control, whereas C-DIM5 decreases MPTP/IFNγ/TNFα -induced gene expression. MPTP/IFNγ/TNFα + C-DIM5 has minimal changes in gene expression compared with control. (n = 4/group in array studies).

including neuronal development and morphogenesis, regulation of cellular differentiation, protein tyrosine kinase activity, and dendritic process development (Fig. 5B). Among these genes, Ppp1r9a, involved in several number of functions including axonogenesis (Nakabayashi et al., 2004) and neuron projection development (Nakanishi et al., 1997), had higher reads per kilobase millions (RPKM) values for p65 binding in the C-DIM5 group, whereas binding of p65 to *Rps6ka3*, involved in Nur77 activation leading to apoptosis, had fewer sequenced reads in treated versus control cells (Fig. 5C).

We also used a targeted qPCR array to identify patterns of mRNA expression in primary astrocytes for 86 NF-κB–regulated genes after treatment with MPTP + TNF/IFN in the presence or absence of C-DIM5 (Fig. 5, D and E). Ontology analysis revealed that the MPTP/TNF/IFN + C-DIM5 group clustered with the control group, distinct from the patterns of gene expression in astrocytes treated with MPTP/TNF/IFN + DMSO (Fig. 5D). A comparison of transcripts differentially expressed between groups ($P < 0.05$) is depicted in Fig. 5E, representing genes involved in inflammation, cell growth, and apoptosis. *Tnf* was the most highly induced transcript in cells treated with MPTP + TNF/IFN, followed by *Ifnb1*, *Birc3*, *Ccl12*, and *Cxcl1* (Fig. 5E, top graph). Each of these genes was downregulated after treatment with MPTP + TNF/IFN in the presence of C-DIM5 (Fig. 5E, middle graph). Comparison of the MPTP + TNF/IFN and control (DMSO) groups indicated little differential expression of transcripts, except for moderate induction of *Tnf* and *Ifng*, albeit at lower levels than in the MPTP+TNF/IFN group (Fig. 5E, lower graph).

Molecular In Silico Modeling Identifies Potential Interactions for C-DIM5 with Both Nur77 and Nurr1. To examine potential differences in C-DIM5 binding affinity between Nur77 and Nurr1, we conducted flexible small-molecule docking studies to predict its binding manner at either the NR4A1 ligand-binding site or the NR4A2 coactivator-binding site. The modeling results indicated that C-DIM5 was predicted to bind with good affinity to NR4A1 (interaction energy: −46.7 kcal/mol), with one of the indole groups buried further into the region of the binding site corresponding to the ligand-binding pocket in a classic nuclear receptor, with both indoles participating in π-alkyl interactions with Leu569 and hydrogen bonds with Glu444 and Asp 593 (Fig. 6). The methoxybenzene moiety was predicted to face toward the exterior of the pocket and form two hydrogen bonds with both the side chain and backbone amines of His515 and a π-cation interaction with Arg514 (Fig. 6, A–C). Additionally, C-DIM5 was predicted to bind the coactivator site of NR4A2 with the para-methoxy substituted benzene of C-DIM5 involved in a hydrogen bond with Lys590, a π-π interaction with Phe439 and hydrophobic interactions with Mse414, whereas the indole moieties participated in both hydrophobic and π-cation interactions with Arg418 (Fig. 6, D–F); however, because of fewer predicted hydrogen bonds and electrostatic interactions compared with NR4A1, the interaction energy was somewhat less favorable (−34.2 vs. −46.7 kcal/mol). Taken together, these data demonstrate that C-DIM5 binds both receptors.

Discussion

Neuronal cell death is accompanied by activation of microglia and astrocytes, resulting in the coordinated expression of multiple NF-κB–regulated inflammatory genes (Verkhratsky and Butt, 2007; Béchade et al., 2014; Murphy and Crean, 2015). In the present study, we demonstrated that a substituted diindolylmethane compound, C-DIM5, inhibits NF-κB in astrocytes through the orphan nuclear receptors, Nur77 and Nurr1. Treatment of astrocytes with C-DIM5 caused an increase in *Nr4a1/Nur77* mRNA without affecting expression of *Nr4a2/Nurr1* (Fig. 1B), suggesting that this compound selectively induces Nur77; these findings were similar to those of studies demonstrating that C-DIM5 transcriptionally activates Nur77 in pancreatic cancer cells (Yoon et al., 2011; Lee et al., 2014). We saw similar results in HEK NF-κB-eGFP-luciferase reporter cells, which express extremely low levels of Nur77 and were refractory to the anti-inflammatory effects of C-DIM5 until transfected with human Nur77 (hNR4A1/TRE-FLAG, Fig. 2). In cells overexpressing Nur77, C-DIM5 inhibited TNF-induced NF-κB activity and increased Nur77 compared with control, suggesting that this compound likely interacts directly with the receptor to stabilize it. Such a specific mechanism of action is supported to be nuclear by the data in Fig. 2, E and F, which demonstrated that C-DIM5 had no effect on nuclear translocation of NF-κB/p65 astrocytes treated with MPTP + TNF/IFN, indicating that inhibition of NF-κB transcriptional activity was not due to interference with upstream activating kinases or to inhibition of nuclear translocation.

In astrocytes treated with MPTP + TNF/IFN, Nur77 redistributed to the cytosol from the nucleus (Fig. 3, A and B). C-DIM5 prevented loss of nuclear Nur77 in astrocytes and similarly increased nuclear levels of Nurr1 (Fig. 3, C and D). This finding is consistent with previous data from our laboratory demonstrating that a related C-DIM (1,1-bis (3′-indolyl)-1-(*p*-chlorophenyl) methane; C-DIM12; chloro-substituted analog) inhibited NF-κB in BV-2 microglial cells by a mechanism involving inhibitory interactions between Nurr1 and p65 at NF-κB transcriptional response elements (De Miranda et al., 2015a). We also separately reported that C-DIM12 increased Nurr1 levels in the nucleus of dopaminergic neurons in the SNpc in mice lesioned with MPTP over 14 days (De Miranda et al., 2013). Thus, the capacity of C-DIM5 to sequester both Nur77 and Nurr1 in the nucleus of astrocytes supports a similar mechanism of inhibition involving receptor-ligand interactions that stabilize the nuclear localization of NR4A1/2. Although Nur77 can translocate to the mitochondria of cancer cells to activate the intrinsic apoptosis pathway through interactions with Bcl-2 family proteins (Lin et al., 2004; Chintharlapalli et al., 2005; Cho et al., 2007; Beard et al., 2015), in normal tissues, Nur77 has anti-inflammatory activity. Studies in cell types ranging from monocytes and T cells to neurons and microglia report that Nurr77 can interact with NF-κB/p65 to limit expression of inflammatory genes (Harant and Lindley, 2004; Li et al., 2015; Murphy and Crean, 2015; Wei et al., 2016; Chen et al., 2017; McEvoy et al., 2017), consistent with the data presented here in primary astrocytes.

To determine whether the inhibitory effects of C-DIM5 on NF-κB–regulated genes required Nur77, we used RNAi directed against Nur77 or Nurr1 in purified astrocyte cultures stimulated with MPTP + TNF/IFN in the presence or absence of C-DIM5 (Fig. 4). Knockdown of either *Nur77* or *Nurr1* resulted in a compensatory increase in mRNA levels for the other receptor (Fig. 4, A and B), whereas knockdown of

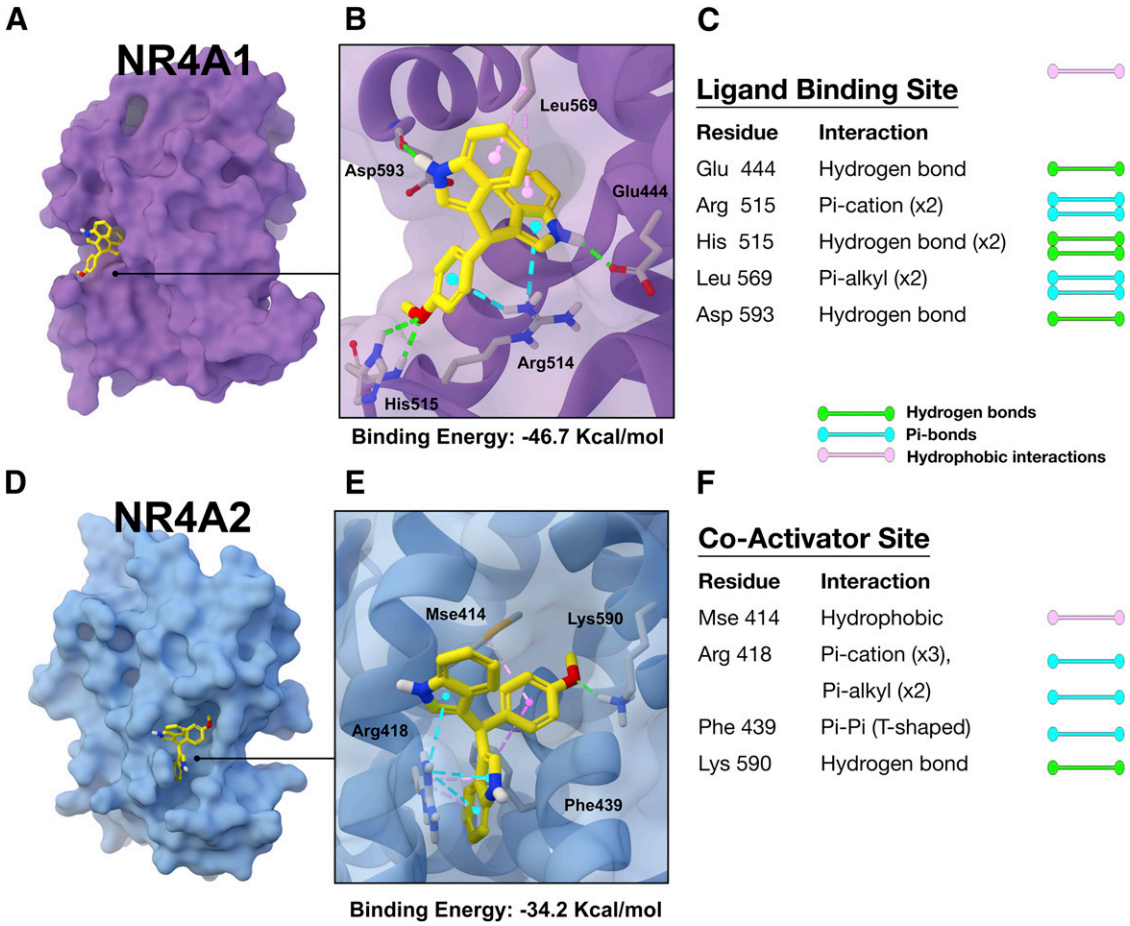

Fig. 6. Small molecule docking of C-DIM5. (A) Predicted binding orientation of C-DIM5 (shown in yellow) at the ligand-binding site of NR4A1 (shown in purple). (B) Inset depicts the specific residues of the calculated binding site in NR4A1 (gray) and their predicted interactions with C-DIM5 as dashed lines (pink=hydrophobic/π-alkyl, purple=π-σ, cyan=π-cation/π-anion, and green=hydrogen bonds). (C) Bond types shown for predicted binding interactions between C-DIM5 and NR4A1. (D) Predicted binding orientation of C-DIM5 (shown in yellow) at the coactivator-binding site of NR4A2 (shown in blue). (E) Inset depicts the specific residues of the calculated binding site in NR4A2 (gray) and their predicted interactions with C-DIM5, with (D) bond types shown for predicted binding interactions between C-DIM5 and NR4A2.

Nr4a3/*Nor1* had no effect on expression of *Nur77* or *Nurr1*. This is a novel observation in astrocytes and suggests that these receptors are transcriptionally coregulated, likely because of the importance of Nur77 and Nurr1 in modulating inflammatory signaling in glial cells. C-DIM5 treatment also selectively increased Nur77 protein levels in astrocytes without altering Nurr1, similar to the effect on *Nurr1* mRNA levels observed in Fig. 1C. When highly purified astrocytes were treated with MPTP + TNF/IFN and C-DIM5, only a modest decrease in inflammatory gene expression resulted (Fig. 4F), likely owing to the absence of microglia and microglial-derived inflammatory factors, which are sensitive to inhibition of inflammatory gene expression by C-DIM compounds (De Miranda et al., 2015a). Knockdown of Nur77 did not prevent the anti-inflammatory effects of C-DIM5 in purified astrocytes, whereas selective knockdown of Nurr1 partially prevented the inhibitory effects of C-DIM5 on inflammatory gene expression; however, double knockdown of both Nur77 and Nurr1 completely abolished the anti-inflammatory effects of C-DIM5 (Fig. 1F, last bar in each graph), supporting a compensatory role for these receptors in regulating inflammatory gene expression in astrocytes, as well as suggesting that C-DIM5 likely acts as a ligand toward both receptors. Because Nurr1 is a potent antagonist of NF-κB–regulated gene expression in macrophages, as well as microglia and astrocytes (Saijo et al., 2009, 2013; De Miranda et al., 2015a), the compensatory increase in expression of Nurr1 that occurs upon knockdown of Nur77 in purified astrocyte cultures therefore likely increased the anti-inflammatory activity of C-DIM5 toward expression of *Nos2*, *Il1b*, *Il6*, and *Tnf* after treatment with MPTP + TNF/IFN, although uncertainty remains in determining the precise role of Nur77 in regulating some of these inflammatory genes that were not significantly induced in pure astrocyte cultures. The favorable binding energies calculated for interactions between C-DIM5 for both Nur77 and Nurr1 (Fig. 6) support such a mechanism of interaction. Taken together with the molecular modeling experiments and nuclear localization data from Fig. 3, these data present strong evidence that C-DIM5 binds and modulates transcriptional activity of both NR4A1/Nur77 and NR4A2/Nurr1 in astrocytes.

Using ChIP-Seq and qPCR array analysis, we identified NF-κB-regulated loci modulated by C-DIM5 (Fig. 5). Venn diagram analysis of ChIP-Seq data identified unique loci bound by p65 after treatment with MPTP + TNF/IFN + C-DIM5, including several important to neuron projection and morphogenesis, as well as regulation of neuronal differentiation and ATP binding (Fig. 5, A and B). Among these,

Ppp1r9a displayed higher RPKM read counts in the MPTP + TNF/IFN + C-DIM5 group, and Rps6ka3 had fewer RPKM read counts after inflammatory stimulus in the presence of C-DIM5 (Fig. 5C). Increased p65 binding to Ppp1r9a (Neuroabin 1) could positively influence the effects of astrocytes on several key cellular functions in neurons, including axonogenesis and actin filament organization (Nakabayashi et al., 2004), as well as neuron projection development (Nakanishi et al., 1997). The positive trophic effects of C-DIM5 were also evident in decreased p65 binding to Rps6ka3 (RSK2), which is involved in the phosphorylation and activation of Nur77 leading to its mitochondrial translocation and loss of its ability to interact with NF-κB/p65 (Wingate et al., 2006; Wang et al., 2009; Kurakula et al., 2014). Thus, C-DIM5 appeared to enhance p65 binding to loci in astrocytes that trophically support neurons while simultaneously decreasing binding of p65 to loci that could enhance inflammation (Harant and Lindley, 2004; Hong et al., 2004; Li et al., 2015).

These findings were further supported by qPCR array data of NF-κB-regulated genes (Fig. 5, D and E), which indicated that transcripts in the MPTP + TNF/IFN+C-DIM5 group statistically clustered with control cells, distinct from gene expression patterns in cells treated only with MPTP+TNF/IFN (Fig. 5D). Numerous differentially expressed inflammatory genes were downregulated by C-DIM5, including *Tnf*, *Stat3*, *Ifnb1*, and complement component *c3*, which is uniquely expressed by activated astrocytes in the central nervous system and correlates closely with a neurotoxic inflammatory phenotype (A1 astrocytes) (Liddelow et al., 2017). *Nr4a2*/*Nurr1*, which is also regulated by NF-κB, was downregulated in both control and MPTP + TNF/IFN groups but upregulated in the MPTP + TNF/IFN + C-DIM5 group. These data support the conclusion that C-DIM5 suppresses inflammatory genes regulated by NF-κB and positively regulates numerous genes important for cell survival and neuronal trophic support.

Computational-based small molecule docking studies predicted binding between C-DIM5 and Nur77 and Nurr1 in either the ligand-binding site or the co-activator binding site, respectively (Fig. 6). Modeling results indicated that C-DIM5 binds with moderately high affinity to the ligand-binding site of Nur77 but also to the co-activator site of Nurr1. Energy minimization data indicate that C-DIM5 likely has binding affinity for both Nur77 and Nurr1 but suggests a greater potency toward Nur77. These findings are in agreement with our previously published data demonstrating that various *para*-phenyl substituted diindolylmethane analogs directly bind Nur77 and modulate its transcriptional activity (Chintharlapalli et al., 2005; Cho et al., 2010; Lee et al., 2014; Safe et al., 2015). Functionally, this suggests that activation of Nur77 and Nurr1 by C-DIM5 globally suppresses the expression of inflammatory genes in primary astrocytes, which is consistent with previous studies from our laboratory indicating that C-DIM5 protects dopamine neurons in mice lesioned with MPTP and prevents inflammatory activation of both microglia and astrocytes in the striatum and substantia nigra (De Miranda et al., 2015b). Given that C-DIM5 has favorable pharmacokinetic distribution to brain following oral dosing (De Miranda et al., 2013), this compound would likely be suitable for further development for small molecule-based approaches targeting neuroinflammation. Collectively, the data presented here suggest that Nur77 and Nurr1 are important modulators of inflammatory signaling in astrocytes that can be pharmacologically targeted to inhibit NF-κB-regulated genes. The specific mechanisms underlying the capacity of C-DIM5 and related compounds to modulate protein-protein and protein-DNA interactions between NR4A receptors and various transcriptional regulatory factors remain to be elucidated.

Acknowledgments

We thank Dr. Dave Carbone for significant guidance and contributions in the early stages of this project and Lindsay Hunt for helpful contributions in Western blotting.

Authorship Contributions

Participated in research design: Popichak, Tjalkens.
Conducted experiments: Popichak, Hammond, Afzali.
Contributed new reagents or analytic tools: Backos, Slayden, Safe.
Performed data analysis: Popichak, Hammond, Moreno, Afzali, Backos.
Wrote or contributed to the writing of the manuscript: Popichak, Hammond, Moreno, Backos, Slayden, Safe, Tjalkens.

References

Aschner M and Kimelberg HK (1991) The use of astrocytes in culture as model systems for evaluating neurotoxic-induced-injury. *Neurotoxicology* **12**:505–517.
Beard JA, Tenga A, and Chen T (2015) The interplay of NR4A receptors and the oncogene-tumor suppressor networks in cancer. *Cell Signal* **27**:257–266.
Béchade C, Colasse S, Diana MA, Rouault M, and Bessis A (2014) NOS2 expression is restricted to neurons in the healthy brain but is triggered in microglia upon inflammation. *Glia* **62**:956–963.
Böhm HJ (1994) The development of a simple empirical scoring function to estimate the binding constant for a protein-ligand complex of known three-dimensional structure. *J Comput Aided Mol Des* **8**:243–256.
Boos DD and Stefanski LA (2011) P-value precision and reproducibility. *Am Stat* **65**: 213–221.
Brooks BR, Brooks CL, III, Mackerell AD, Jr, Nilsson L, Petrella RJ, Roux B, Won Y, Archontis G, Bartels C, Boresch S, et al. (2009) CHARMM: the biomolecular simulation program. In *J. Comput. Chem* **30**:1545–1614.
Carbone DL, Popichak KA, Moreno JA, Safe S, and Tjalkens RB (2009) Suppression of 1-methyl-4-phenyl-1,2,3,6-tetrahydropyridine-induced nitric-oxide synthase 2 expression in astrocytes by a novel diindolylmethane analog protects striatal neurons against apoptosis. *Mol Pharmacol* **75**:35–43.
Chen Y, Jin Y, Zhan H, Chen J, Chen Y, Meng H, Jin J, Yu L, Cao X, and Xu Y (2017) Proteomic analysis of the effects of Nur77 on lipopolysaccharide-induced microglial activation. *Neurosci Lett* **659**:33–43.
Chintharlapalli S, Burghardt R, Papineni S, Ramaiah S, Yoon K, and Safe S (2005) Activation of Nur77 by selected 1,1-Bis(3′-indolyl)-1-(*p*-substituted phenyl) methanes induces apoptosis through nuclear pathways. *J Biol Chem* **280**: 24903–24914.
Cho SD, Lee SO, Chintharlapalli S, Abdelrahim M, Khan S, Yoon K, Kamat AM, and Safe S (2010) Activation of nerve growth factor-induced B alpha by methylene-substituted diindolylmethanes in bladder cancer cells induces apoptosis and inhibits tumor growth. *Mol Pharmacol* **77**:396–404.
Cho SD, Yoon K, Chintharlapalli S, Abdelrahim M, Lei P, Hamilton S, Khan S, Ramaiah SK, and Safe S (2007) Nur77 agonists induce proapoptotic genes and responses in colon cancer cells through nuclear receptor-dependent and nuclear receptor-independent pathways. *Cancer Res* **67**:674–683.
De Miranda BR, Miller JA, Hansen RJ, Lunghofer PJ, Safe S, Gustafson DL, Colagiovanni D, and Tjalkens RB (2013) Neuroprotective efficacy and pharmacokinetic behavior of novel anti-inflammatory para-phenyl substituted diindolylmethanes in a mouse model of Parkinson's disease. *J Pharmacol Exp Ther* **345**:125–138.
De Miranda BR, Popichak KA, Hammond SL, Jorgensen BA, Phillips AT, Safe S, and Tjalkens RB (2015a) The Nurr1 activator 1,1-Bis(3′-Indolyl)-1-(p-Chlorophenyl) Methane blocks inflammatory gene expression in BV-2 microglial cells by inhibiting nuclear factor κB. *Mol Pharmacol* **87**:1021–1034.
De Miranda BR, Popichak KA, Hammond SL, Miller JA, Safe S, and Tjalkens RB (2015b) Novel para-phenyl substituted diindolylmethanes protect against MPTP neurotoxicity and suppress glial activation in a mouse model of Parkinson's disease. *Toxicol Sci* **143**:360–373.
Feig M, Onufriev A, Lee MS, Im W, Case DA, and Brooks CL III (2004) Performance comparison of generalized born and Poisson methods in the calculation of electrostatic solvation energies for protein structures. *J Comput Chem* **25**:265–284.
Flaig R, Greschik H, Peluso-Iltis C, and Moras D (2005) Structural basis for the cell-specific activities of the NGFI-B and the Nurr1 ligand-binding domain. *J Biol Chem* **280**:19250–19258.
Frakes AE, Ferraiuolo L, Haidet-Phillips AM, Schmelzer L, Braun L, Miranda CJ, Ladner KJ, Bevan AK, Foust KD, Godbout JP, et al. (2014) Microglia induce motor neuron death via the classical NF-κB pathway in amyotrophic lateral sclerosis. *Neuron* **81**:1009–1023.

Harant H and Lindley IJ (2004) Negative cross-talk between the human orphan nuclear receptor Nur77/NAK-1/TR3 and nuclear factor-kappaB. *Nucleic Acids Res* **32**:5280–5290.
Hirsch EC, Breidert T, Rousselet E, Hunot S, Hartmann A, and Michel PP (2003) The role of glial reaction and inflammation in Parkinson's disease. *Ann N Y Acad Sci* **991**:214–228.
Hirsch EC and Hunot S (2000) Nitric oxide, glial cells and neuronal degeneration in parkinsonism. *Trends Pharmacol Sci* **21**:163–165.
Hong CY, Park JH, Ahn RS, Im SY, Choi HS, Soh J, Mellon SH, and Lee K (2004) Molecular mechanism of suppression of testicular steroidogenesis by proinflammatory cytokine tumor necrosis factor alpha. *Mol Cell Biol* **24**:2593–2604.
Jain AN (1996) Scoring noncovalent protein-ligand interactions: a continuous differentiable function tuned to compute binding affinities. *J Comput Aided Mol Des* **10**:427–440.
Jankovic J (2008) Parkinson's disease: clinical features and diagnosis. *J Neurol Neurosurg Psychiatry* **79**:368–376.
Kalia LV and Lang AE (2015) Parkinson's disease. *Lancet* **386**:896–912.
Karin M and Ben-Neriah Y (2000) Phosphorylation meets ubiquitination: the control of NF-[kappa]B activity. *Annu Rev Immunol* **18**:621–663.
Kirkley KS, Popichak KA, Afzali MF, Legare ME, and Tjalkens RB (2017) Microglia amplify inflammatory activation of astrocytes in manganese neurotoxicity. *J Neuroinflammation* **14**:99.
Koska J, Spassov VZ, Maynard AJ, Yan L, Austin N, Flook PK, and Venkatachalam CM (2008) Fully automated molecular mechanics based induced fit protein-ligand docking method. *J Chem Inf Model* **48**:1965–1973.
Kurakula K, Koenis DS, van Tiel CM, and de Vries CJ (2014) NR4A nuclear receptors are orphans but not lonesome. *Biochim Biophys Acta* **1843**:2543–2555.
Lee S-O, Li X, Hedrick E, Jin U-H, Tjalkens RB, Backos DS, Li L, Zhang Y, Wu Q, and Safe S (2014) Diindolylmethane analogs bind NR4A1 and are NR4A1 antagonists in colon cancer cells. *Mol Endocrinol* **28**:1729–1739.
Li L, Liu Y, Chen HZ, Li FW, Wu JF, Zhang HK, He JP, Xing YZ, Chen Y, Wang WJ, et al. (2015) Impeding the interaction between Nur77 and p38 reduces LPS-induced inflammation. *Nat Chem Biol* **11**:339–346.
Liddelow SA, Guttenplan KA, Clarke LE, Bennett FC, Bohlen CJ, Schirmer L, Bennett ML, Münch AE, Chung WS, Peterson TC, et al. (2017) Neurotoxic reactive astrocytes are induced by activated microglia. *Nature* **541**:481–487.
Lin B, Kolluri SK, Lin F, Liu W, Han YH, Cao X, Dawson MI, Reed JC, and Zhang XK (2004) Conversion of Bcl-2 from protector to killer by interaction with nuclear orphan receptor Nur77/TR3. *Cell* **116**:527–540.
Livak KJ and Schmittgen TD (2001) Analysis of relative gene expression data using real-time quantitative PCR and the 2(-delta delta C(T)) method. *Methods* **25**: 402–408.
McEvoy C, de Gaetano M, Giffney HE, Bahar B, Cummins EP, Brennan EP, Barry M, Belton O, Godson CG, Murphy EP, et al. (2017) NR4A receptors differentially regulate NF-κB signaling in myeloid cells. *Front Immunol* **8**:7.
Murphy EP and Crean D (2015) Molecular interactions between NR4A orphan nuclear receptors and NF-κB are required for appropriate inflammatory responses and immune cell homeostasis. *Biomolecules* **5**:1302–1318.
Nakabayashi K, Makino S, Minagawa S, Smith AC, Bamforth JS, Stanier P, Preece M, Parker-Katiraee L, Paton T, Oshimura M, et al. (2004) Genomic imprinting of PPP1R9A encoding neurabin I in skeletal muscle and extra-embryonic tissues. *J Med Genet* **41**:601–608.
Nakanishi H, Obaishi H, Satoh A, Wada M, Mandai K, Satoh K, Nishioka H, Matsuura Y, Mizoguchi A, and Takai Y (1997) Neurabin: a novel neural tissue-specific actin filament-binding protein involved in neurite formation. *J Cell Biol* **139**: 951–961.
Panneton WM, Kumar VB, Gan Q, Burke WJ, and Galvin JE (2010) The neurotoxicity of DOPAL: behavioral and stereological evidence for its role in Parkinson disease pathogenesis. *PLoS One* **5**:e15251.
Parrill AL and Reddy MR (1999) Rational Drug Design: Novel Methodology and Practical Applications, American Chemical Society, Washington, DC.
Pekny M and Nilsson M (2005) Astrocyte activation and reactive gliosis. *Glia* **50**: 427–434.
Pekny M, Wilhelmsson U, and Pekna M (2014) The dual role of astrocyte activation and reactive gliosis. *Neurosci Lett* **565**:30–38.
Qin C, Morrow D, Stewart J, Spencer K, Porter W, Smith R, III, Phillips T, Abdelrahim M, Samudio I, and Safe S (2004) A new class of peroxisome proliferator-activated receptor gamma (PPARgamma) agonists that inhibit growth of breast cancer cells: 1,1-Bis(3′-indolyl)-1-(p-substituted phenyl)methanes. *Mol Cancer Ther* **3**:247–260.
Rothe T, Ipseiz N, Faas M, Lang S, Perez-Branguli F, Metzger D, Ichinose H, Winner B, Schett G, and Krönke G (2017) The nuclear receptor Nr4a1 acts as a microglia rheostat and serves as a therapeutic target in autoimmune-driven central nervous system inflammation. *J Immunol* **198**:3878–3885.
Safe S, Jin UH, Morpurgo B, Abudayyeh A, Singh M, and Tjalkens RB (2015) Nuclear receptor 4A (NR4A) family—orphans no more. J Steroid Biochem Mol Biol 157: 48–60.
Saijo K, Crotti A, and Glass CK (2013) Regulation of microglia activation and deactivation by nuclear receptors. *Glia* **61**:104–111.
Saijo K, Winner B, Carson CT, Collier JG, Boyer L, Rosenfeld MG, Gage FH, and Glass CK (2009) A Nurr1/CoREST pathway in microglia and astrocytes protects dopaminergic neurons from inflammation-induced death. *Cell* **137**:47–59.
St-Hilaire M, Bourhis E, Lévesque D, and Rouillard C (2006) Impaired behavioural and molecular adaptations to dopamine denervation and repeated L-DOPA treatment in Nur77-knockout mice. *Eur J Neurosci* **24**:795–805.
Tanaka M, Fuentes ME, Yamaguchi K, Durnin MH, Dalrymple SA, Hardy KL, and Goeddel DV (1999) Embryonic lethality, liver degeneration, and impaired NF-kappa B activation in IKK-beta-deficient mice. *Immunity* **10**:421–429.
Teismann P and Schulz JB (2004) Cellular pathology of Parkinson's disease: astrocytes, microglia and inflammation. *Cell Tissue Res* **318**:149–161.
Verkhratsky A and Butt A (2007) Glial Neurobiology: A Textbook, John Wiley & Sons Ltd., New York.
Wang A, Rud J, Olson CM, Jr, Anguita J, and Osborne BA (2009) Phosphorylation of Nur77 by the MEK-ERK-RSK cascade induces mitochondrial translocation and apoptosis in T cells. *J Immunol* **183**:3268–3277.
Wang Z, Benoit G, Liu J, Prasad S, Aarnisalo P, Liu X, Xu H, Walker NPC, and Perlmann T (2003) Structure and function of Nurr1 identifies a class of ligand-independent nuclear receptors. *Nature* **423**:555–560.
Wei X, Gao H, Zou J, Liu X, Chen D, Liao J, Xu Y, Ma L, Tang B, Zhang Z, et al. (2016) Contra-directional coupling of Nur77 and Nurr1 in neurodegeneration: a novel mechanism for memantine-induced anti-inflammation and anti-mitochondrial impairment. *Mol Neurobiol* **53**:5876–5892.
Wingate AD, Campbell DG, Peggie M, and Arthur JSC (2006) Nur77 is phosphorylated in cells by RSK in response to mitogenic stimulation. *Biochem J* **393**:715–724.
Wu G, Robertson DH, Brooks CL III, and Vieth M (2003) Detailed analysis of grid-based molecular docking: a case study of CDOCKER-A CHARMm-based MD docking algorithm. *J Comput Chem* **24**:1549–1562.
Yoon K, Lee SO, Cho SD, Kim K, Khan S, and Safe S (2011) Activation of nuclear TR3 (NR4A1) by a diindolylmethane analog induces apoptosis and proapoptotic genes in pancreatic cancer cells and tumors. *Carcinogenesis* **32**:836–842.

Address correspondence to: Dr. Ronald Tjalkens, Professor of Toxicology and Neuroscience, Department of Environmental and Radiological Health Sciences, College of Veterinary Medicine and Biomedical Sciences, Colorado State University, 1680 Campus Delivery, Physiology Building, Room 101, Fort Collins, CO 80523-1680. E-mail: ron.tjalkens@colostate.edu